Spectrochimica Acta Part A 81 (2011) 53–58

Contents lists available at ScienceDirect

Spectrochimica Acta Part A: Molecular and Biomolecular Spectroscopy

journal homepage: www.elsevier.com/locate/saa

Combustion synthesis, characterization and Raman studies of ZnO nanopowders

A. Jagannatha Reddy[a], M.K. Kokila[b], H. Nagabhushana[c,*], J.L. Rao[d], C. Shivakumara[e], B.M. Nagabhushana[f], R.P.S. Chakradhar[g,**]

[a] Department of Physics, M. S. Ramaiah Institute of Technology, Bangalore 560054, India
[b] Department of Physics, Bangalore University, Bangalore 560056, India
[c] C.N.R. Rao Centre for Advanced Materials Research, Tumkur University, Tumkur 572103, India
[d] Department of Physics, S.V. University, Tirupathi 517502, India
[e] Solid State and Structural Chemistry Unit, Indian Institute of Science, Bangalore 560012, India
[f] Department of Chemistry, M. S. Ramaiah Institute of Technology, Bangalore 560054, India
[g] National Aerospace Laboratories (CSIR), Bangalore 560017, India

ARTICLE INFO

Article history:
Received 10 February 2011
Received in revised form 10 May 2011
Accepted 16 May 2011

Keywords:
ZnO
Combustion synthesis
XRD
SEM
TEM
FTIR
UV–vis
Raman spectroscopy

ABSTRACT

Spherical shaped ZnO nanopowders (14–50 nm) were synthesized by a low temperature solution combustion method in a short time <5 min. Rietveld analysis show that ZnO has hexagonal wurtzite structure with lattice constants $a = 3.2511(1)$ Å, $c = 5.2076(2)$ Å, unit cell volume $(V) = 47.66(5)$ (Å)^3 and belongs to space group P63mc. SEM micrographs reveal that the particles are spherical in shape and the powders contained several voids and pores. TEM results also confirm spherical shape, with average particle size of 14–50 nm. The values are consistent with the grain sizes measured from Scherrer's method and Williamson–Hall (W–H) plots. A broad UV–vis absorption spectrum was observed at ~375 nm which is a characteristic band for the wurtzite hexagonal pure ZnO. The optical energy band gap of 3.24 eV was observed for nanopowder which is slightly lower than that of the bulk ZnO (3.37 eV). The observed Raman peaks at 438 and 588 cm^{-1} were attributed to the E_2 (high) and E_1 (LO) modes respectively. The broad band at 564 cm^{-1} is due to disorder-activated Raman scattering for the A_1 mode. These bands are associated with the first-order Raman active modes of the ZnO phase. The weak bands observed in the range 750–1000 cm^{-1} are due to small defects.

1. Introduction

In the recent decade, semiconductor nano particles have received considerable attention, due to its unique quantum nature, which changes the material solid state properties [1]. Therefore, the synthesis and study of nanostructure materials have become current topic of research worldwide. It is well known that many fundamental properties of nanostructure materials can be expressed as a function of their size, composition and structural order. Meanwhile, nanostructures with different morphologies are nuclear parts of functional nanostructure devices [2,3]. Among various technologically important materials, the wide and direct band gap (3.37 eV) II–VI semiconductor ZnO has rapidly emerged as a promising optoelectronic material especially due to its low power threshold for optical pumping at room temperature, highly efficient UV emission resulting from a large exciton binding energy at room temperature (60 meV). This large exciton binding energy provides excitonic emission more efficiently even at higher temperature. Due to its wide bandgap, ZnO is transparent in the visible part of the electromagnetic spectrum and can therefore be used as a transparent conducting oxide [4], UV-sensitive and solar-blind photodetector [5], shield against high-energy radiation [6], organic light-emitting diodes (O-LED) [7] and transparent thin-film transistors (TTFT) [8]. Some of the field-effect transistors even use ZnO nanorods as conducting channels [9,10]. Thus wurtzite structured ZnO has practical benefits that make it an attractive material from an industrial point of view.

ZnO material with various shapes, such as spherical nano particles, nanotubes, nanoribbons, nanowires, nanobelts, tripods, hexagonal columns, hollow spheres, nanoneedles, mushrooms, snowflakes and so on have aroused much interest [11–16]. Various techniques have been used to prepare these materials and among them solid state method is frequently used. The conventional way of producing these materials in large scale is by the solid-state reaction method. The solid-state reaction method has some inherent disadvantages such as: (i) chemical inhomogeneity, (ii) coarser particle size, and (iii) introduction of impurities during ball milling, etc. To achieve better quality nanostructured materials low temperature synthesizing procedure is desired. Obviously

* Corresponding author.
** Corresponding author. Tel.: +91 080 2508 6251.
E-mail address: sreechakra72@yahoo.com (R.P.S. Chakradhar).

1386-1425/$ – see front matter © 2011 Elsevier B.V. All rights reserved.
doi:10.1016/j.saa.2011.05.043

at higher temperature, the grain growth is strongly stimulated and particles grow to sizes beyond nano-regime.

As a part of our programme on nanomaterials, here we report the preparation of spherical shaped nanocrystalline ZnO powders (14–50 nm) by a low temperature solution combustion method [17,18]. The combustion reaction is initiated in a muffle furnace at temperatures less than 400 °C or much lower than the phase transition of the target material. The synthesized nano powders are well characterized for their structure using Powder X-ray diffraction (PXRD). The morphological studies were carried out using scanning electron microscopy (SEM) and transmission electron microscopy (TEM). In addition the specific surface area (BET); Fourier transformed infrared (FTIR), UV–vis and Raman spectroscopy (RS) were employed to investigate nanopowders and the results are discussed in detail.

2. Material and methods

2.1. Synthesis of ZnO nanoparticles

The synthesis process involved the combustion of redox mixtures in which zinc nitrate [$Zn(NO_3)_2$,$6H_2O$] acted as an oxidizing reactant and oxalyl di-hydrazide (ODH) [$C_2H_6N_4O_2$] as a reducing one. The initial composition of solution containing Zinc nitrate and ODH was calculated based on the total oxidizing and reducing valences of the oxidizer and the fuel using the concepts of propellant chemistry [19]. All the reagents were of analytical purity, and used without further purification. Zinc nitrate and ODH were mixed with minimum quantity of doubled distilled water in a cylindrical petri dish and stirred for few minutes until clear solution is formed. The dish was introduced into a muffle furnace maintained at 300 °C. The solution initially undergoes dehydration, followed by decomposition with the evolution of large amounts of gases. The mixture then froths and swells forming foam, which ruptures with a flame and glows to incandescence. During incandescence the foam further swells to the capacity of the container. The entire combustion process is over in 5 min. The foam was grinded to obtain fine powder of ZnO.

The reaction for combustion synthesis in the present case can be written as follows:

$$Zn(NO_3)_2 + C_2H_6N_4O_2 \rightarrow ZnO + 3N_2 + 2CO + 3H_2O$$

2.2. Instruments used

The powder X-ray diffraction (PXRD) studies were carried out using Phillips X-ray diffractometer (model PW 3710) with Cu Kα radiation (λ = 1.5405 Å). The surface morphology of the samples was examined using SEM (JEOL JSM 840A) by sputtering technique with gold as covering contrast material. TEM analysis was performed on a Hitachi H-8100 (accelerating voltage up to 200 kV, LaB_6 filament) equipped with EDS (Kevex Sigma TM Quasar, USA). The FTIR studies have been performed on a Perkin Elmer Spectrometer (Spectrum 1000) with KBr pellets. The UV–vis spectrum was recorded on a UV-3101 Shimadzu Visible spectrometer. Raman studies were carried out on Renishaw *In-via* Raman spectrometer with 633 nm He–Cd laser and a Leica DMLM optical microscope equipped with 50× objective, thus providing a laser spot of 2 μm in diameter. Specific surface area of the powders was measured using Quanta chrome corporation, NOVA 1000 gas sorption analyzer.

3. Results and discussion

3.1. Powder X-ray diffraction studies (PXRD)

Fig. 1 shows the PXRD of as-formed and calcined (500, 700, 900 and 1000 °C for 2 h) ZnO samples. The three strongest XRD peaks for

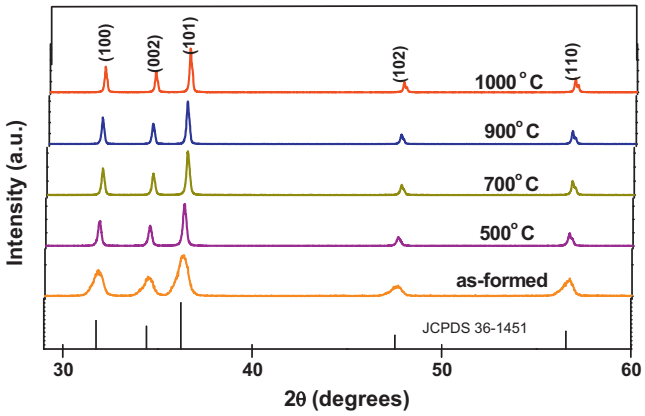

Fig. 1. PXRD patterns of as-formed and heat treated ZnO.

ZnO were detected with Miller indices (1 0 0), (0 0 2) and (1 0 1) corresponding to Bragg angles 31.8°, 34.5° and 36.4° respectively. All diffraction peaks can be readily indexed to wurtzite hexagonal ZnO structure with lattice constants $a = 3.2511(1)$ Å and $c = 5.2076(2)$ Å, consistent with the standard PDF database (JCPDS file No. 36-1451). The characteristic peaks are higher in intensity which indicates that the products are of good crystalline nature. No peaks corresponding to impurities are detected, showing that the final product is purely ZnO. It is observed that intensity of the peaks increases with thermal treatment due to agglomeration, which means that the crystallinity has been improved. The full width at half maxima (FWHM) of major peaks decreases and confirms the grain size growth. The average crystallite size was estimated from the Debye–Scherrer's equation:

$$D = \frac{k\lambda}{\beta \cos\theta} \quad (1)$$

where β is FWHM (rad), λ is wavelength of X-rays, θ is diffraction angle. The average crystallite size (D) was found to be in the range 14–50 nm.

The lattice parameters for hexagonal ZnO nanoparticles were estimated from the equation:

$$\frac{1}{d^2} = \frac{4}{3(h^2 + hk + k^2/a^2)} + \frac{l^2}{c^2} \quad (2)$$

where a and c are the lattice parameters and h, k, and l are the Miller indices and $d_{h\,k\,l}$ is the interplaner spacing for the plane ($h\,k\,l$). This interplaner spacing can be calculated from Bragg's law:

$$2d \sin\theta = n\lambda \quad (3)$$

The volume (V) of the unit cell for hexagonal system and the number of unit cells (n) in the particle (considering it to be spherical in shape) have been calculated from the following equations:

$$V = 0.866 \times a^2 \times c \quad (4)$$

$$n = \frac{4}{3\pi(D/2V)} \quad (5)$$

where D is the average particle size. Significant extent of strains are associated with nanoparticles because they are known to have a number of surface atoms which have unsaturated in co-ordinations. We have estimated and compared the strains in as-formed and calcined ZnO nanoparticles using the W–H equation [20]:

$$\beta \cos\theta = \frac{k\lambda}{D} + 4\varepsilon \sin\theta \quad (6)$$

where ε is the strain associated with the nanoparticles.

Eq. (6) represents a straight line between $4\sin\theta$ (X-axis) and $\beta\cos\theta$ (Y-axis). The slope of line gives the strain (ε) and inter-

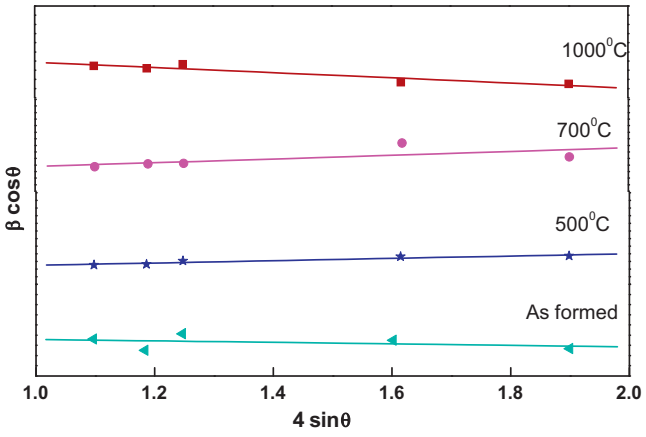

Fig. 2. Williamson–Hall plots of as-formed and heat treated ZnO.

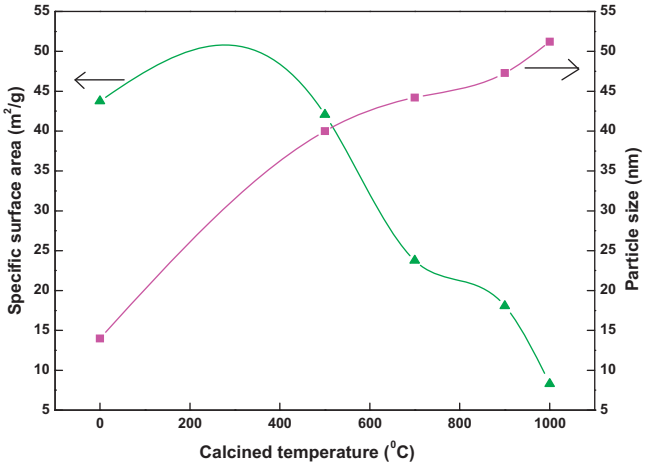

Fig. 3. Variation of BET surface area and particle size with calcined temperature.

cept ($k\lambda/D$) of this line on Y-axis gives grain size (D). Fig. 2 shows the W–H plots of as-formed and calcined samples. It is observed that the strain present in as-formed sample is more when compared to calcined samples, indicating the reduction in the number of surface atoms with increase in temperature. This is because, the crystallinity, particle size and number of unit cells present in particle increases with heat treatment. Effective crystallite size (D) for as-formed ZnO nanoparticles is 14 nm, however upon calcination at 1000 °C it increases to 51 nm. The specific surface area measured by Brunauer, Emmett and Teller (BET) method, decreases from 43.7 m^2/g for as-formed ZnO nanoparticles to 23.7 m^2/g for 1000 °C calcined sample. Fig. 3 shows the variation of specific surface area and the particle size with temperature. The data obtained accordingly are given in Table 1.

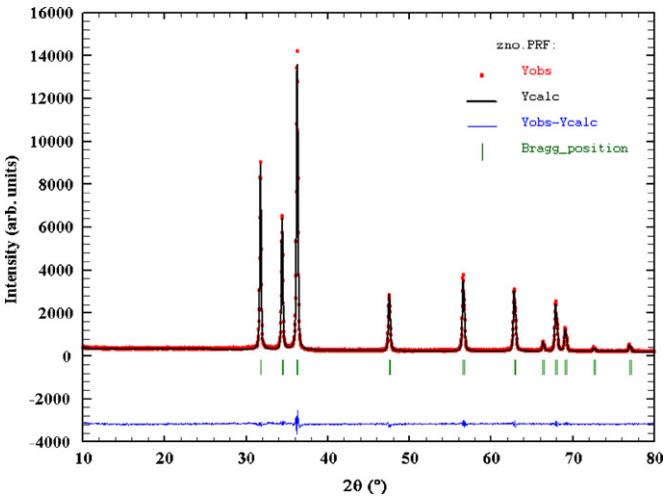

Fig. 4. Reitveld analysis of ZnO (as formed).

The Rietveld refinement is a method in which the profile intensities obtained from step-scanning measurements of the powders allow to estimate an approximate structural model for the real structure. This was performed with a FULLPROF program [21]. By utilizing the pseudo-voigt function in order to fit the several parameters to the data point: one scale factor, one zero shifting, four back ground, three cell parameters, five shape and width of the peaks, one global thermal factor and two asymmetric factors. A typical Rietveld analysis of the as-formed ZnO sample is shown in Fig. 4 which presents the experimental and calculated PXRD patterns obtained by the refinement of ZnO. The corresponding packing diagram is shown in Fig. 5. The refined parameters such as occupancy, atomic functional positions are listed in Table 2. The fitting parameters (R_p, R_{wp} and χ^2) indicate a good agreement between the refined and observed PXRD patterns for the wurtzite ZnO. The refined lattice parameter values $a = 3.2511(1)$ Å, $c = 5.2076(2)$ Å and cell volume $(V) = 47.66(5)$ (Å)^3 confirm that ZnO has a hexagonal structure.

3.2. Scanning electron microscopy (SEM)

Fig. 6 shows the SEM micrographs of as-formed and calcined ZnO nanopowders at different temperature (500, 700, 900 and 1000 °C). It is observed that the circular shaped primary particles are agglomerated with varying sizes in the range 40–50 nm. Here, the particle size was greatly dependent on the calcination temperature. As calcination temperature increases the size also increases, due to congregation effect, which is reflected in surface area and PXRD measurements. SEM micrographs show the pores and voids in the sample, which can be attributed to the large amount of gases escaping out of the reaction mixture during the combustion.

Table 1
Crystallite size, BET surface area, lattice parameters and strain of as-formed and calcined ZnO nanocrystals.

Temp. (°C)	Crystallite size (nm) by Scherrer's formula	Crystallite size (nm) from W–H plot	Lattice parameters (Å)		Volume of unit cell (Å)^3	No. of unit cells in particle ($\times 10^4$)	BET surface area (m^2/g)	Strain ($\times 10^{-4}$)
			a	c				
As-formed	14	14.47	3.229	5.273	47.62	3.15	43.76	15.4
500	40	42.66	3.227	5.271	47.56	7.75	42.06	11.8
700	44.2	46.67	3.222	5.262	47.33	10.3	23.76	9.7
1000	51.2	49.34	3.220	5.258	47.22	13.8	8.28	6.8

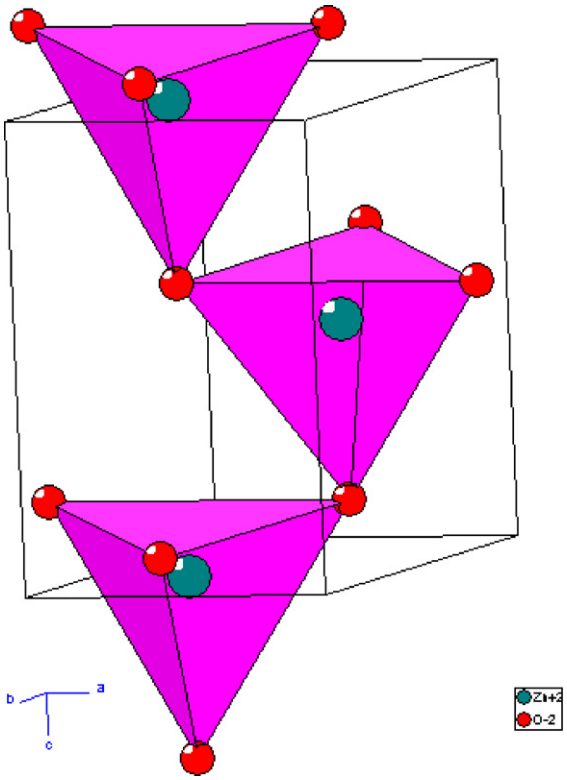

Fig. 5. Packing diagram of ZnO.

3.3. Transmission electron microscopy (TEM)

The typical TEM micrograph of as-formed ZnO nanoparticles is shown in Fig. 7. As seen in TEM image, the sample consists of spherical shaped particles with varying sizes ranging 10–50 nm. In the selective area diffraction (SAED) pattern, clear bright spots representing crystal planes of hexagonal ZnO are visible. This in addition to the XRD spectra in Fig. 1, confirms that the ZnO nanoparticles are highly crystalline with hexagonal structure. The particle sizes measured from TEM are in good agreement to those measured from Powder X-ray diffraction patterns and Williamson–Hall plots.

3.4. Fourier transformed infrared spectroscopy (FTIR)

Fig. 8 shows FTIR spectrum of the as-formed and calcined ZnO nanocrystalline samples at different temperatures (500, 700, 900 and 1000 °C for 2 h). The peaks at ~3400 and 1626 cm^{-1} are attributed to O–H stretching vibration and H–O–H bending vibration respectively, which are assigned to small amount of H_2O existing in the nanocrystalline ZnO. The peak at 435 cm^{-1} is ascribed to Zn–O stretching vibration [22,23]. A small peak at 1350 cm^{-1} is due to a weak nitrite group, which might have resulted from the nitrate group being adsorbed on the ZnO powder surface. The 3400, 1626 and 1300 cm^{-1} peaks are not observed in 700 and 900 °C calcined samples due to decomposition of H_2O and nitrate groups.

3.5. Raman spectroscopy

Raman scattering measurement was performed to investigate the vibrational properties of the ZnO nanostructures at room temperature. Raman is very sensitive and non destructive tool for investigating semiconductor nanostructures. The wurtzite-phase ZnO belongs to the space group P63mc with two formula units per primitive cell. The irreducible representation at the zone-center is $2A_1 + 2E_1 + 2B_1 + 2E_2$. One A_1 and one E_1 modes are acoustic phonons and the remaining modes are optical phonons. In the optical phonons, A_1 and E_1 are polar modes, B_1 is a silent mode and E_2 is a non-polar mode. Group theory predicts that there are two A_1, two E_1, two E_2 and two B_1 modes. Only the two B_1 modes are not Raman active. In case of highly *C*-axis oriented ZnO, if the incident light is exactly normal to the surface, only A_1(LO) and E_2 mode can be observed. The other modes are forbidden according to the Raman selection rules [24]. Fig. 9 shows the room-temperature Raman spectrum of ZnO, with several peaks at 100, 332, 438, 564 and 588 cm^{-1}, which are attributed to optical phonons of ZnO. The intense and fairly narrow peak at 438 cm^{-1} corresponds to a non-polar optical phonon E_2 (high) of wurtzite ZnO while the 332 cm^{-1} is assigned to the second-order Raman spectrum arising from zone-boundary phonons of the hexagonal ZnO [25]. The low intense Raman bands in the region from 1150–1400 cm^{-1} are attributed to the optical overtones and associated with the second-order Raman active modes [26]. The peak at 564 cm^{-1} is attributed to the A_1(LO) mode of the hexagonal ZnO. Some other peaks at position 1434, 1576 and 1663 cm^{-1} are also observed in ZnO sample. Origins of these peaks are not clear at the present moment.

3.6. UV–visible spectrum and optical energy gap (E_g)

UV–vis spectroscopy has been used to study the absorption characteristics of as-formed ZnO nano particles. Fig. 10 shows the room temperature UV–vis absorption spectrum of the ZnO nanopowder. A broad band at ~375 nm was observed in the spectrum which is a characteristic band for the wurtzite hexagonal pure ZnO. No other peaks were observed in the spectrum which confirms that the as synthesized product is ZnO only. Figure illustrates the UV–vis absorption spectrum of the nanoparticles which has a red shift (375 nm) compared to that of the bulk ZnO (~370 nm). This red shift can be explained by the formation of shallow levels inside the band gap due to impurity atoms present in the lattice. Quantum size effects on electronic energy bands of semiconductors become more prominent when the size of the nano crystallites is less than the bulk exciton Bohr radius. Coulomb interaction between hole and electron plays a crucial role in nanosized solids. The quantum confinement of charge carriers modifies valence and conduction bands of semiconductors. The optical energy gap E_g of un-doped ZnO was estimated using the Tauc relation [27]

$$\alpha(h\nu) \sim (h\nu - E_g)^{1/n} \quad (7)$$

Table 2
Rietveld refinement results and atomic co-ordination employed to model as-formed ZnO unit cell.

System: ZnO	Space group: P63mc (186)	
a = 3.2511(1) Å	c = 5.2076(2) Å	V = 47.66(5) (Å)^3
R_{Bragg} = 3.05	R_p = 4.29	R_{wp} = 5.64,
R_F = 2.20,	χ^2 = 1.55	

Atom	Oxidation state	Wyckoff notation	x	y	z	Occupancy
Zn	+2	2b	0.3333	0.6666	0.0000	1
O	−2	2b	0.3333	0.6666	0.3809(8)	1

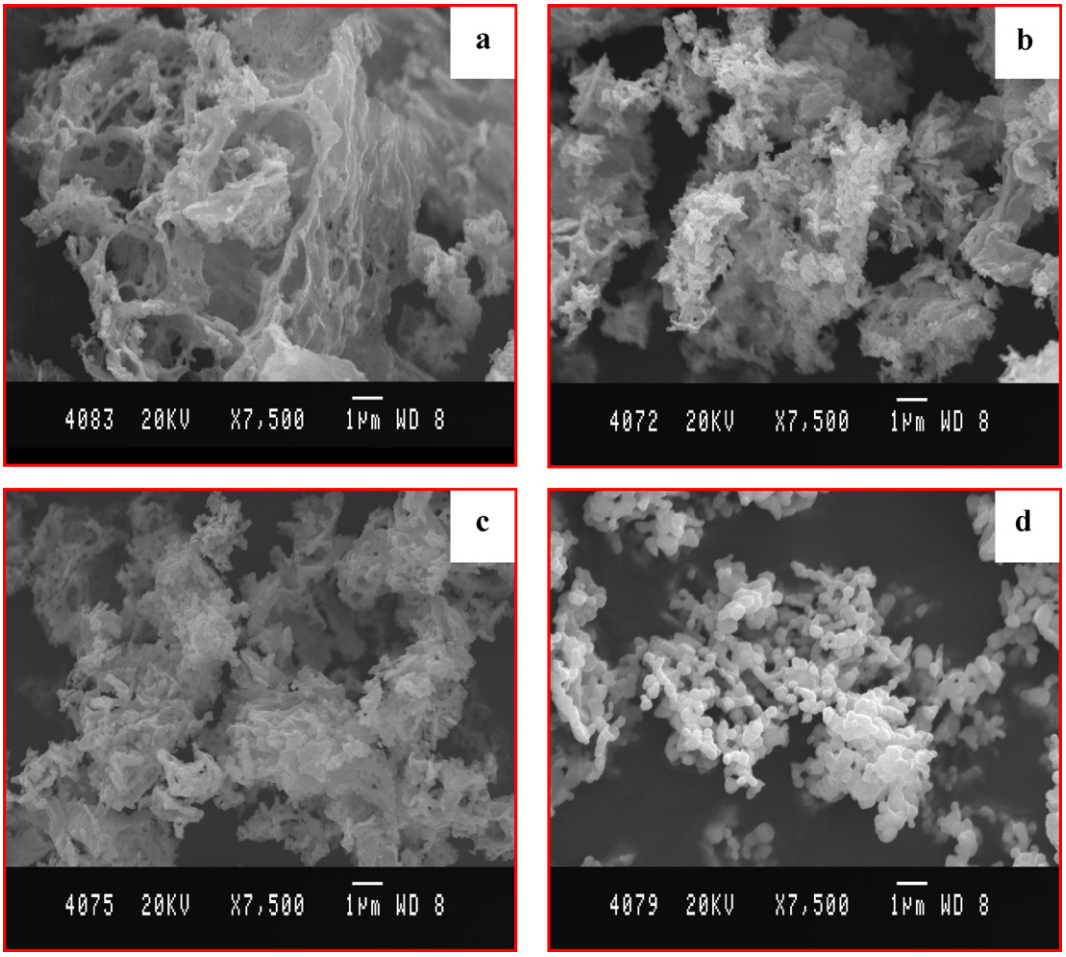

Fig. 6. SEM micrographs of ZnO powders (a) as-formed (b) heat-treated at 500 °C (c) 700 °C (d) 1000 °C.

where $h\nu$ is the photon energy and α is the optical absorption coefficient near the fundamental absorption edge. The absorption coefficients were calculated from the optical absorption spectra. The optical band gap of ZnO is obtained by plotting $(\alpha E)^n$ versus E in the high-absorption range followed by extrapolating the linear region of the plots to $(\alpha E)^n = 0$ (Fig. 10, inset). The analysis of present data showed that, the plots give linear relations which can for the most part be fitted with the above equation with $n = 2$ indicating that allowed direct transitions are responsible for the interband transitions in the sample. From the figure it is seen that the sample has an optical energy band gap of 3.24 eV that is slightly lower than that of the bulk ZnO (3.37 eV). This red shift may be attributed to the agglomeration occurring in the sample. This agreement is suggested by SEM micrographs.

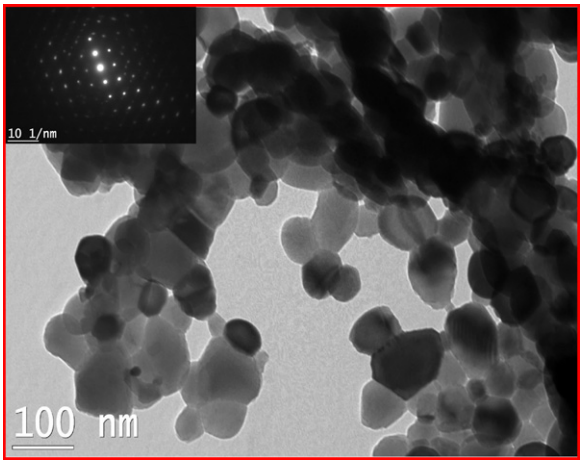

Fig. 7. TEM micrographs of as-formed ZnO powder (inset) SAED pattern.

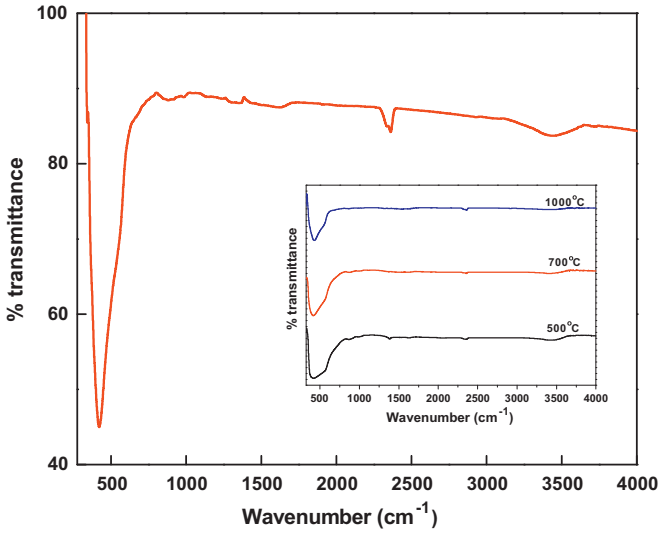

Fig. 8. FTIR spectrum of as-formed ZnO (inset) FTIR of heat treated ZnO.

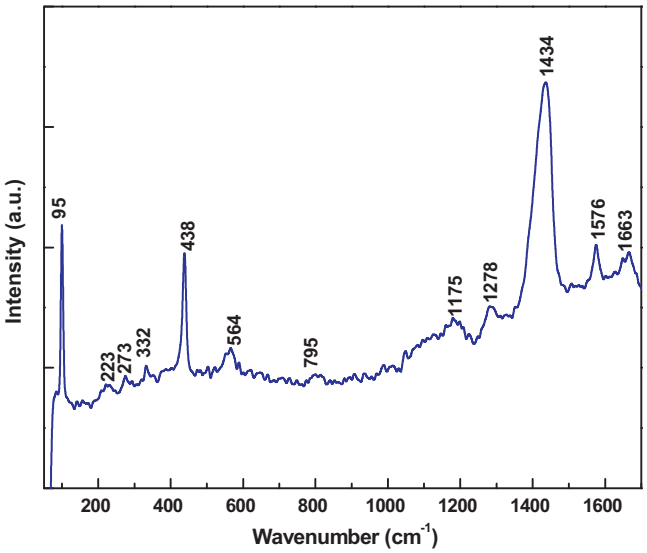

Fig. 9. Raman spectrum of as-formed ZnO.

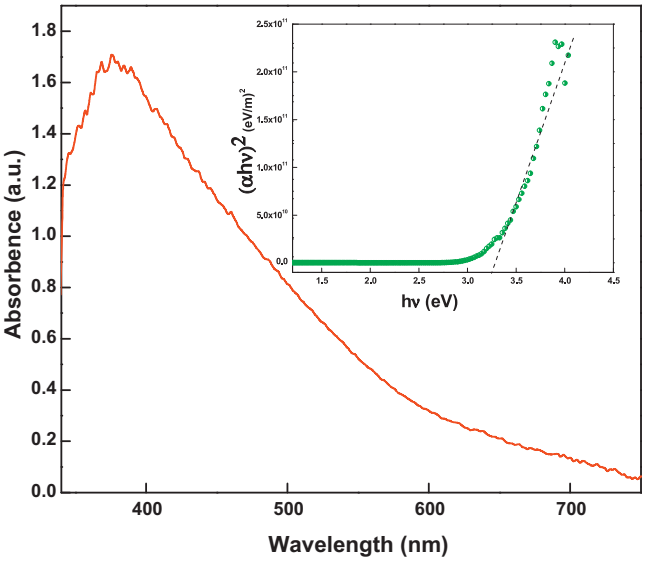

Fig. 10. UV–vis absorption spectrum of as-formed ZnO (inset) plot of $(\alpha h\gamma)^2$ versus $(h\nu)$.

4. Conclusions

ZnO nanoparticles have been synthesized by cost effective low temperature solution combustion method in a short time. PXRD profiles confirmed that the structures of the prepared products are Wurtzite structure without any secondary phases. The average particle size of the synthesized powder determined by Debye–Scherrer's formula is found to be in the range 14–51 nm which was confirmed by W–H plots and TEM results. The crystallinity increases when calcined to high temperatures. SEM profiles show the product is porous with voids, spongy and agglomeration. Raman studies indicate first and second order active modes of ZnO phase. Optical energy band gap of nanocrystals is slightly lower than that of the bulk ZnO.

Acknowledgements

Dr. B.M. Nagabhushana gratefully acknowledges Visvesvaraya Technological University, Belgaum, for the financial support (VTU/2009-10/A-9/11714) to carryout this research work. Dr. H. Nagabhushana thanks Dr. S.C. Sharma, Vice-chancellor, Tumkur University, Tumkur, for constant encouragement and support. A. Jagannatha Reddy expresses his gratitude to Dr. M. Suguna, for fruitful discussions regarding nanomaterials.

References

[1] Y. Wang, N. Herron, J. Phys. Chem. 95 (1991) 525–532.
[2] X.M. Sun, X. Chen, Z.X. Deng, Y.D. Li, Mater. Chem. Phys. 78 (2002) 99–104.
[3] R. Turgeman, S. Tirosh, A. Gedanken, Chem. Eur. J 10 (2004) 1845–1850.
[4] C. Agashe, O. Kluth, G. Schope, H. Siekmann, J. Hupkes, B. Rech, Thin Solid Films 442 (2002) 167.
[5] P. Sharma, A. Mansingh, K. Sreenivas, Appl. Phys. Lett. 80 (2002) 553–555.
[6] D.C. Look, D.C. Reynolds, J.W. Hemsky, R.L. Jones, J.R. Sizelove, Appl. Phys. Lett. 75 (1999) 811–813.
[7] P. Gorrn, T. Rabe, W. Kowalsky, F. Galbrecht, U. Scherf, Appl. Phys. Lett. 89 (2006) 161113.
[8] J. Nishii, A. Ohtomo, K. Ohtani, H. Ohno, M. Kawasaki, Jpn. J. Appl. Phys. 44 (2005) L1193–L1195.
[9] H.J. Kim, C.-H. Lee, D.-W. Kim, G.-C. Yi, Nanotechnology 17 (2006) S327–S331.
[10] K. Koike, I. Nakashima, K. Hashimoto, S. Sasa, M. Inoue, M. Yano, Appl. Phys. Lett. 87 (2005) 112106–112108.
[11] L. Zhang, Y. Ding, M. Povey, D. York, Prog. Nat. Sci. 18 (2008) 939–944.
[12] J. Xie, H. Deng, Z.Q. Xu, Y. Li, J. Huang, J. Cryst. Growth 292 (2006) 227–229.
[13] C. Liewhiran, S. Phanichphant, Sensors 7 (2007) 650–675.
[14] A. Sasaki, W. Hara, A. Mastuda, N. Tateda, K. Saitom, M. Yoshimoto, Appl. Phys. Lett. 86 (2005) 231911–231921.
[15] M.K. Patra, K. Manzoor, M. Manoth, S.R. Vadera, N. Kumar, J. Lumin. 128 (2008) 267–272.
[16] L. Vayssieres, Adv. Mater. 15 (2003) 464–466.
[17] J.J. Kingsley, K.C. Patil, Mater. Lett. 6 (1988) 427–432.
[18] B.M. Nagabhushana, R.P.S. Chakradhar, K.P. Ramesh, V. Prasad, C. Shivakumara, G.T. Chandrappa, Phil. Mag. 90 (2010) 2009–2025.
[19] S. Ekambaram, N. Arul Dhas, K.C. Patil, Int. J. Self-prop. High-temp. Synth. 4 (1995) 85–93.
[20] G.K. Willamson, W.H. Hall, Acta Metall. 1 (1953) 22–31.
[21] J. Rodrigueg-carvajal, Fullprof. 2000: a program for Rietveld, profile matching and integrated intensity refinements for X-ray and neutron data. Version 1.6. Laboratorie Leon, Brillounin, Gifsuryvette, France, 2009.
[22] A. Kajbafvala, M.R. Shayegh, M. Mazloumi, S. Zanganeh, S.K. Aidin Lak, Sadrnezhaad, J. Alloys Compd. 469 (2009) 293–297.
[23] M. Ristic, S. Musiĭc, M. Ivanda, S. Popovĭic, J. Alloys Compd. 397 (2005) L1–L4.
[24] A. Fonoberov, A.A. Balandin, Phys. Rev. B 70 (2004) 233205–233208.
[25] K.A. Alim, V.A. Fonoberov, M. Shamsa, A.A. Balandina, J. Appl. Phys. 97 (2005) 124313–124323.
[26] G.J. Exarhos, S.K. Sharma, Thin Solid Films 270 (1995) 27–32.
[27] H. Nagabhushana, B.M. Nagabhushana, M. Kumar, H.B. Premkumar, C. Shivakumara, R.P.S. Chakradhar, Phil. Mag. 26 (2010) 3567–3579.